

# PROJECTION METHOD FOR DROPLET DYNAMICS ON GROOVE-TEXTURED SURFACE WITH MERGING AND SPLITTING

YUAN GAO

*Department of Mathematics, Duke University, Durham, NC*

JIAN-GUO LIU

*Department of Mathematics and Department of Physics, Duke University, Durham, NC*

**ABSTRACT.** We study the full dynamics of droplets placed on an inclined groove-textured surface with merging and splitting. The motion of droplets can be determined by the contact line dynamics and motion by mean curvature, which are driven by the competition between surfaces tensions of three phases and gravitational effect. We reformulate the dynamics as a gradient flow on a Hilbert manifold with boundary, which can be further reduced to a parabolic variational inequality under some differentiable assumptions. To efficiently solve the parabolic variational inequality, the convergence and stability of projection method for obstacle problem in Hilbert space is revisited using Trotter-Kato's product formula. Based on this, we proposed a projection scheme for the droplets dynamics, which incorporates both the obstacle information and the phase transition information when merging and splitting happen. Several challenging examples including splitting and merging of droplets are demonstrated.

## 1. INTRODUCTION

Let us start from an abstract Cauchy problem in Hilbert space  $X$  with the standard norm and inner product, denoted as  $\|\cdot\|$ ,  $\langle \cdot, \cdot \rangle$  respectively,

$$(1.1) \quad \partial_t u(t) \in -\partial\varphi(u(t)) \quad \text{for a.e. } t > 0, u(0) = u_0,$$

where  $\partial\varphi$  is the subdifferential of a convex functional  $\varphi : X \rightarrow \mathbb{R} \cup \{\pm\infty\}$  with effective domain  $D(\varphi) := \{u \in X; \varphi(u) < +\infty\}$ . Assume  $\varphi$  is bounded below,  $\lambda$ -convex and lower semi-continuous in  $X$ . Then for any  $u_0 \in \overline{D(\varphi)}^{\|\cdot\|}$ , there exists a unique mild solution to (1.1) [23, 4] expressed by the continuous nonlinear semigroup on  $[0, +\infty)$  of contraction, which is generated by  $\partial\varphi$  and denoted as  $S(t)$  (or symbolic notation  $S(t) = e^{-t\partial\varphi}$ ). The mild solution is also known as evolutionary variational inequality (EVI) solution [2] in the sense that

$$(1.2) \quad \langle u - v, u_t \rangle = \frac{1}{2} \frac{d}{dt} \|u(t) - v\|^2 \leq \varphi(v) - \varphi(u(t)), \quad \text{for a.e. } t > 0, \forall v \in D(\varphi).$$

---

*E-mail addresses:* [yuangao@math.duke.edu](mailto:yuangao@math.duke.edu), [jliu@math.duke.edu](mailto:jliu@math.duke.edu).

*Date:* December 4, 2021.

One method to solve (1.1) is to construct the minimizing movement sequence [4, 2] at each time  $t^k := k\tau$  (then make piecewise constant interpolation)

$$(1.3) \quad u^{k+1} = \operatorname{argmin}_{u \in X} \varphi(u) + \frac{\|u - u^k\|^2}{2\tau},$$

which is equivalent to

$$(1.4) \quad u^{k+1} = (I + \tau \partial \varphi)^{-1} u^k =: J_\tau^{\partial \varphi} u^k,$$

where  $J_\tau^{\partial \varphi}$  is called the resolvent operator of  $\partial \varphi$ . The convergence theory for the minimizing movement sequence is general, particularly for the case  $\partial \varphi$  is multi-valued. However, it is usually hard to compute the resolvent since it involves global information of  $\varphi$  rather than local derivatives of  $\varphi$ .

For one special case that the Gâteaux derivatives, denoted as  $\nabla \varphi$ , of  $\varphi$  exists, i.e.  $\partial \varphi$  is single-valued, then the original problem (1.1) is reduced to a standard PDE problem instead of EVI problem. However, for a class of problems, for instance the Cauchy problem (1.1) with some constraint, the Gâteaux derivative of  $\varphi$  does not exist for the whole space. More precisely, let  $K$  be a closed convex subset in Hilbert Space  $X$  and we seek solution  $u(t) \in K$  to (1.1) for any  $t \geq 0$ . Assume the convex functional  $\varphi$  has the following special form

$$(1.5) \quad \varphi = E + I_K, \quad E : X \rightarrow \mathbb{R} \text{ is Gâteaux differentiable, } I_K(x) := \begin{cases} 0, & x \in K; \\ +\infty, & x \notin K. \end{cases}$$

In this case, one can either follow theory of EVI solution to still consider the problem in  $X$

$$(1.6) \quad \partial_t u(t) \in -\partial(E + I_K)(u(t)), \quad \text{for a.e. } t > 0, u(0) = u_0,$$

Alternatively, to take the advantage of the efficient local information from Gâteaux derivatives  $\nabla E$ , one can consider an equivalent parabolic variational inequality (PVI)

$$(1.7) \quad \langle v - u(t), -\partial_t u(t) \rangle \leq \langle v - u(t), \nabla E \rangle, \quad \text{for a.e. } t > 0, \forall v \in K.$$

Following the convention, when Gâteaux derivatives exist, we refer (1.7) as parabolic variational inequality (PVI) to distinguish from the more general case using subdifferential, i.e. EVI (1.6). Although this is still an inequality, there are various methods to approximate this weak formulation and to solve the discretized system; c.f. [17].

To further convert the inequality to an equality, the  $L^2$  penalty method for the obstacle problem with  $K := \{u \in L^2; u \geq w\}$  is introduced by [17, 30] and recently an advanced  $L^1$  penalty method is introduced by [32, 40]. They replace the indicator function  $I_K(u)$  in the total energy by a  $L^2$  (resp.  $L^1$ ) penalty  $\mu \|(g - u)_+\|_{L^2}$  (resp.  $\mu \|(w - u)_+\|_{L^1}$ ) with a large enough parameter  $\mu$ . Although the penalty parameter  $\mu$  brings additional stiffness, the  $L^1$  penalty is easy to implement and adapt to other implicit schemes for the whole problem [32].

In this paper, we focus on the projection method (a.k.a fractional/splitting method [25]) for a class of problems with constraint, especially for obstacle problems. The projection method splits the problem into two steps, gradient flow  $\partial_t u = -\nabla E$  and projection to  $K$ , which are conducted iteratively. The projection method is particularly efficient when the projection step has a closed formula or is easy to implement. For instance, the projection method is used to solve incompressive Navier-Stokes equation [9, 31]; see also projection method for the Landau-Lifshitz equation [36].

For the typical obstacle problem with  $K := \{u \in L^2; u \geq w\}$ , the projection operator has the explicit formula

$$(1.8) \quad \text{Proj}_K(u) = \max\{u, w\}.$$

We revisit Trotter-Kato's product formula for nonlinear maximal monotone operator [21], and use it to propose a projection method for the droplet dynamics with merging and splitting. To approximate  $u(t^k)$  at  $t^k = k\tau = k\frac{T}{n}$ , the 1st order projection method construct the iterative sequence  $u^k$  as follows.

$$(1.9) \quad u^{k+1} = (I + \tau \partial I_K)^{-1} (I + \tau \nabla E)^{-1} u^k = \text{Proj}_K(I + \tau \nabla E)^{-1} u^k.$$

We will give details for the projection method in Section 2, whose convergence to the EVI solution to (1.6) is ensured by Trotter-Kato's product formula.

Based on abstract observations above, we now focus on the dynamics of volume preserving droplets placed on an impermeable groove-textured surface. The dynamics of a liquid drop with capillary effect is essentially a mean curvature flow associated with free boundaries due to the impermeable groove-textured substrate. In addition to the pure mean curvature flow indicating the motion of an interface between two phases, the leading driven force for droplet dynamics is the contact line dynamics. The dynamic contact angle tends to go to the equilibrium contact angle (a.k.a Young's angle) which is determined by the competitions between surface tension coefficients of three phases at the contact lines; see Section 3.1.2.

The dynamics of droplets is a historical but challenging problem due to the geometric complexity. On one hand, for the quasi-static dynamics, i.e. the capillary surface is determined by an elliptic equation, there are many analysis results on the global existence and homogenization problems; see [5, 19, 22, 14] for capillary surface described by a harmonic equation and see [6, 7, 8, 15] for capillary surface described by spatial-constant mean curvature equation. On the other hand, for the pure mean curvature flow with an obstacle but without contact line dynamics, we refer to [1, 26] for local existence and uniqueness of a regular solution by constructing a minimizing movement sequence.

Instead, we study the gradient flow formulation on a Hilbert manifold with boundary and numerical simulations for the full dynamics of droplets described by the combination of contact line dynamics and mean curvature flow of the capillary surface. The dynamics become more complicated due to gravitational effect, constantly changed slope of the groove-textured surface, and the unavoidable topological changes such as splitting and merging. Using the gradient flow formulation in metric space, we will describe the droplets dynamics as a trajectory on a Hilbert manifold  $\mathcal{M}$  with boundary brought by the obstacle. This can be regarded as an extension of the constrained (obstacle) problem (1.6) from the Hilbert space  $X$  to the Hilbert manifold  $\mathcal{M}$ . Similarly, taking the advantage of the directional differentiability of the free energy on the Hilbert manifold  $\mathcal{M}$ , we further reformulate the problem as a PVI problem (3.34), which can be used to describe the topological changes of droplets during time evolution; see Section 3.2.

However, the pure PVI formulation misses the phase transition information at the splitting (merging) point where interface between two phases becomes a triple junction between three phases. Hence pure PVI is not enough to correctly show the physical phenomena. Indeed, the droplets are

not allowed to move along the boundary of the manifold any more after splitting into two parts. Therefore, we propose a projection scheme in Section 4.1 to incorporate both obstacle information and phase transition information. The projection scheme is built upon the unconditionally stable 1st/2nd numerical schemes for single 2D droplet dynamics developed by the authors [16], which efficiently decouple the boundary updates from the capillary surface update using an unconditionally stable explicit 1D boundary moving. Although the convergence of the projection scheme is only proved in Hilbert space, the projection method still works efficiently since we have the explicit formula for the projection operator to  $\mathcal{M}$ . Several numerical simulations are conducted in Section 4.2 including the splitting of one droplet on an inclined groove-textures substrate and the merging of two droplets in a Utah teapot. There are also many other numerical methods for simulating the dynamics of droplets, c.f. [24, 27, 39, 13, 12, 34] and the references therein. Especially, in [20, 35], with local treatments at the splitting point, the author simulate the pinch off of solid drops described by surface diffusion with either sharp interface dynamics or the corresponding phase field model.

The remaining part of the paper will be organized as follows. In Section 2, we study the convergence and stability of the abstract projection method in Hilbert space. In Section 3, we derive the gradient flow on Hilbert manifold in EVI/PVI version for droplets dynamics with merging and splitting. In Section 4, based on the abstract theory of the projection method, we propose the projection method for gradient flow on Hilbert manifold in PVI version to incorporate the obstacle information and phase transition information and conduct several numerical simulations including merging and splitting of droplets on groove-textured surfaces.

## 2. CONVERGENCE AND STABILITY OF PROJECTION METHOD IN HILBERT SPACE

In this section, we revisit the abstract theory of projection method for gradient flows in Hilbert space, whose convergence is ensured by Trotter-Kato's product formula [21]. Let  $X = L^2(\mathbb{R}^d)$  be a Hilbert space,  $K := \{u \in L^2(\mathbb{R}^d); u \geq w\}$  and  $I_K$  be the indicator function of  $K$  defined in (1.5). Assume

$$(2.1) \quad \begin{aligned} E : X \rightarrow \mathbb{R} &\text{ is convex, l.s.c functional on } X; \\ E &\text{ is Gâteaux differentiable with Gâteaux derivative } \nabla E. \end{aligned}$$

Consider the obstacle problem (1.6). Since  $A + B = \partial(E + I_K)$  is maximal monotone operator in  $X$ ,  $A + B$  generates a strongly continuous semigroup on  $[0, +\infty)$  of contractions [23, 4], denoted as  $S(t) := e^{-t\partial(E+I_K)}$ . For any  $u_0 \in K$ , the mild solution to (1.6) is given by

$$(2.2) \quad u(t) = e^{-t\partial(E+I_K)}u_0.$$

We revisit the first order projection method for the nonlinear problem (1.6) below. For  $\tau := \frac{T}{n}$ , we use projection method to construct an approximation  $u^k$  of  $u(t^k)$  with  $t^k = k\tau$  below.

Step (i) For  $u^k \in K$ , find

$$(2.3) \quad \tilde{u}^{k+1} = \operatorname{argmin}_{u \in X} E(u) + \frac{\|u - u^k\|^2}{2\tau};$$

which is equivalent to

$$(2.4) \quad \tilde{u}^{k+1} = (I + \tau \nabla E)^{-1}u^k;$$

Step (ii) Find  $u^{k+1}$  as

$$(2.5) \quad u^{k+1} = \text{Proj}_K(\tilde{u}^{k+1}) = \max\{\tilde{u}^{k+1}, w\},$$

which is equivalent to

$$(2.6) \quad \tilde{u}^{k+1} - u^{k+1} \in \tau \partial I_K(u^{k+1}),$$

due to  $\partial I_K$  is a convex cone.

Rewrite the Step (ii) as

$$(2.7) \quad u^{k+1} = (I + \tau \partial I_K)^{-1} \tilde{u}^{k+1}.$$

In summary, we have

$$(2.8) \quad u^{k+1} = (I + \tau \partial I_K)^{-1} (I + \tau \nabla E)^{-1} u^k.$$

Denote  $A := \nabla E$ ,  $B := \partial I_K$ . The corresponding resolvent operators of  $A$  and  $B$  are denoted as  $J_\tau^A := (I + \tau \nabla E)^{-1}$  and  $J_\tau^B := (I + \tau \partial I_K)^{-1}$  respectively. The projection method above can be recast as

$$(2.9) \quad u^{k+1} = J_\tau^B J_\tau^A u^k.$$

Next, to obtain the approximated solution  $\bar{u}_n(t)$  at any  $t \in [0, T]$ , we use the piecewise constant interpolation from  $u^k$  with  $\tau = \frac{T}{n}$  such that

$$(2.10) \quad \bar{u}_n(t) \equiv u^k, \quad t \in [k\tau, (k+1)\tau),$$

which is equivalent to

$$(2.11) \quad \bar{u}_n(t) := (J_{\frac{T}{n}}^B J_{\frac{T}{n}}^A)^{[\frac{nt}{\tau}]} u_0, \quad t \in [0, T].$$

**Theorem 2.1** (Convergence Theorem [21]). *Let  $t \in [0, T]$  and  $u(t)$  be the mild solution of (1.6). Let  $\bar{u}_n(t)$  in (2.11) be the numeric solution obtained from projection method with time step  $\tau = \frac{T}{n}$ . Then we have the convergence*

$$(2.12) \quad \lim_{n \rightarrow +\infty} \sup_{t \in [0, T]} \|\bar{u}_n(t) - u(t)\| = 0.$$

*Proof.* The proof is to directly apply Trotter-Kato's product formula [21].

First, since  $A + B = \partial(E + I_K)$  is maximal monotone operator in  $X$ ,  $A + B$  generates a strongly continuous semigroup on  $[0, +\infty)$  of contractions, denoted symbolically as  $S(t) := e^{-t\partial(E+I_K)}$ . For any  $u_0 \in K$ , the mild solution to (1.6) is given by

$$(2.13) \quad u(t) = e^{-t\partial(E+I_K)} u_0.$$

Second, recall the resolvent of  $A$  and  $B$  are  $J_\tau^A = (I + \tau \nabla E)^{-1}$  and  $J_\tau^B = (I + \tau \partial I_K)^{-1}$  respectively. We use Trotter-Kato's product formula [21] to prove

$$(2.14) \quad u^n(t) := \left( J_{\frac{T}{n}}^B J_{\frac{T}{n}}^A \right)^n u_0 \rightarrow u(t), \quad \text{as } n \rightarrow +\infty, \quad \text{uniformly for } t \geq 0.$$

To see this, in [21] we take  $U_1 := J_{\frac{T}{n}}^A$ ,  $U_2 := J_{\frac{T}{n}}^B$ . Then by [21, Example 2.3], we know  $U_1$  are a nice  $E$ -family with index  $\gamma \geq 2$  and  $U_2$  are a nice  $I_K$ -family with index  $\gamma \geq 2$ . Hence the condition (i) in [21, Theorem] holds, which gives the claim (2.14).

Finally, for the projection scheme for  $t \in [0, T]$  with time step  $\tau = \frac{T}{n}$ , the piecewise constant interpolation in  $[k\tau, (k+1)\tau]$  is given by

$$(2.15) \quad \bar{u}_n(t) = (J_\tau^B J_\tau^A)^{[\frac{t}{\tau}]} u_0, \quad t \in [0, T],$$

where  $[a]$  is the integer part of real number  $a$ . Since  $\tau[\frac{t}{\tau}] \rightarrow t$  as  $n \rightarrow +\infty$ , we know

$$(2.16) \quad u(\tau[\frac{t}{\tau}]) \rightarrow u(t)$$

due to continuous semigroup property. Therefore we conclude

$$(2.17) \quad \|\bar{u}_n(t) - u(t)\| \leq \|(J_\tau^B J_\tau^A)^{[\frac{t}{\tau}]} u_0 - u(\tau[\frac{t}{\tau}])\| + \|u(\tau[\frac{t}{\tau}]) - u(t)\| \rightarrow 0$$

as  $n \rightarrow +\infty$  uniformly in  $t \in [0, T]$ . □

**2.1. Second order projection method.** Furthermore, using the middlepoint scheme, we also propose the second order projection method below and prove its stability. For  $\tau := \frac{T}{n}$ , we use projection method to construct an approximation  $u^k$  of  $u(t^k)$  with  $t^k = k\tau$  below.

Step (I) Using the middle-point scheme to find  $\tilde{u}^k$  such that

$$(2.18) \quad \frac{\tilde{u}^{k+1} - u^k}{\tau} = -\nabla E\left(\frac{\tilde{u}^{k+1} + u^k}{2}\right);$$

Step (II) Find  $u^{k+1}$  as

$$(2.19) \quad u^{k+1} = \text{Proj}_K(\tilde{u}^{k+1}).$$

Denote  $v^{k+1} := \frac{\tilde{u}^{k+1} + u^k}{2}$ . The Step (I) above is equivalent to

$$(2.20) \quad 2(v^{k+1} - u^k) = -\tau \nabla E(v^{k+1}).$$

This can also be interpreted as constructing minimizing movement

$$(2.21) \quad v^{k+1} = \underset{v \in X}{\text{argmin}} E(v) + \frac{1}{\tau} \|v - u^k\|^2.$$

Recall  $A = \nabla E$ ,  $B = \partial I_K$  and the corresponding Resolvent operators are  $J_\tau^A = (I + \tau \nabla E)^{-1}$ ,  $J_\tau^B = (I + \tau \partial I_K)^{-1}$  respectively. (2.20) can be recast as

$$(2.22) \quad v^{k+1} = J_{\frac{\tau}{2}}^A u^n = (I + \frac{\tau}{2} A)^{-1} u^n.$$

Therefore, Step (I) above is to find

$$(2.23) \quad \tilde{u}^{k+1} = 2v^{k+1} - u^k = (2J_{\frac{\tau}{2}}^A - I)u^k = (I - \frac{\tau}{2} A)(I + \frac{\tau}{2} A)^{-1} u^k.$$

In summary, the second order projection method is

$$(2.24) \quad u^{k+1} = J_\tau^B (2J_{\frac{\tau}{2}}^A - I)u^k = (I + \tau B)^{-1} (I - \frac{\tau}{2} A)(I + \frac{\tau}{2} A)^{-1} u^k.$$

**Lemma 2.2.** *Suppose there exists  $u^*$  such that  $J_\tau^B (2J_{\frac{\tau}{2}}^A - I)u^* = u^*$ . Then we have*

$$(2.25) \quad \|u^{k+1} - u^*\| \leq \|u^k - u^*\|.$$

*Proof.* Since  $A, B$  are monotone operators, both  $J_\tau^B$  and  $J_\tau^A$  are firmly nonexpansive, i.e.

$$\|Jx - Jy\|^2 + \|(x - y) - (Jx - Jy)\|^2 \leq \|x - y\|^2.$$

Thus we know  $2J_\tau^A - I$  is nonexpansive. Therefore we have

$$(2.26) \quad \|u^{k+1} - u^*\| = \|J_\tau^B(2J_\tau^A - I)u^k - J_\tau^B(2J_\tau^A - I)u^*\| \leq \|(2J_\tau^A - I)u^k - (2J_\tau^A - I)u^*\| \leq \|u^k - u^*\|.$$

□

### 3. GRADIENT FLOW FORMULATION OF DROPLET DYNAMICS WITH MERGING AND SPLITTING

In this section, we describe the droplets dynamics with topological changes via gradient flow formulations. We first give the kinematic description of a volume preserving droplet via potential flow in Section 3.1.1. Then in Section 3.1.2 and Section 3.1.3 we study the driven energy and the dissipation mechanism of the droplets dynamics using the purely geometric configuration: contact domain and capillary surface. Finally, with the specific free energy  $\mathcal{F}$  on manifold  $\mathcal{M}$  and dissipation relation described by a Riemannian metric, in Section 3.2 we derive the gradient flow formulation in EVI/PVI version.

**3.1. Droplets dynamics as purely geometric motions.** We study the motion of a three-dimensional droplet placed on an impermeable substrate  $\{(x, y, z); z = 0\}$ . Let the wetting domain (a.k.a. contact domain) be  $(x, y) \in D \subset \mathbb{R}^2$  with boundary  $\Gamma := \partial D$ . We focus on the case that droplet is described a graph function  $u(x, y)$ ; physically known as capillary surface. The droplet domain is then identified by the area

$$A := \{(x, y, z); (x, y) \in D, 0 < z < u(x, y), u|_{\partial D} = 0\}$$

with sharp interface. We will give the kinematic description, driven energy and dissipation mechanism in this section.

**3.1.1. Kinematic description of a droplet via potential flow.** Assume the fluid inside the droplet is an incompressible potential flow with velocity  $v(x, y, z) = \nabla\phi(x, y, z)$  and constant density  $\rho$ . To completely describe the motion of a droplet described above, we need to clarify the following three kinematic boundary conditions. (i) The motion of  $\Gamma$  (physically known as contact lines) with outer normal  $n_{cl}$  in  $x$ - $y$  plane is described by the contact line speed

$$(3.1) \quad v_{cl} := n_{cl} \cdot \nabla_{x,y}\phi(x, y, 0), \quad (x, y) \in \Gamma;$$

(ii) the motion of the capillary surface on  $\partial A \cap \{z > 0\}$  with the outer normal  $n$  is described by the normal speed

$$(3.2) \quad v_n := n \cdot \nabla\phi, \quad (x, y, z) \in \partial A \cap \{z > 0\},$$

and (iii) there is no penetration on the impermeable substrate, so  $v_n = 0$  on  $\partial A \cap \{z = 0\}$ . With these kinematic boundary conditions and  $\nabla \cdot v = 0$ , the incompressible potential flow can be uniquely solved from

$$(3.3) \quad \begin{aligned} \Delta\phi &= 0, \quad x \in A(t) \\ \partial_n\phi &= \begin{cases} v_n, & x \in \partial A(t) \cap \{u > 0\}, \\ 0, & x \in \partial A(t) \cap \{u = 0\}. \end{cases} \end{aligned}$$

The compatibility condition  $\int_{\partial A} v_n \, ds = 0$ , is ensured by the volume preserving constraint. Indeed, notice

$$(3.4) \quad \int_{\partial A} v_n \, ds = \int_{D(t)} \frac{\partial_t u}{\sqrt{1 + |\nabla u|^2}} \sqrt{1 + |\nabla u|^2} \, dx \, dy = \int_{D(t)} \partial_t u \, dx \, dy,$$

where we used the normal speed  $v_n = \frac{\partial_t u}{\sqrt{1 + |\nabla u|^2}}$  in the graph representation. Then by  $u(x, y, t) = 0$  on  $\Gamma(t)$  and the Reynolds transport theorem, we have

$$(3.5) \quad \int_{D(t)} \partial_t u \, dx \, dy = \frac{d}{dt} \int_{D(t)} u(x, y, t) \, dx \, dy = 0,$$

where the last equality follows from the volume preserving constraint  $\frac{d}{dt} \int_{D(t)} u(x, y, t) \, dx \, dy = 0$ . Hence in the volume preserving case, the motion of the droplet can be completely described by the motion of capillary surface  $u(x, y, t)$  and the motion of contact domain  $D(t)$ .

**3.1.2. Free energy for the droplet and Young's angle.** Now we clarify the free energy of a droplet following the notations and terminologies in the classical book of De Gennes [11]. For a droplet placed on a substrate, surface tension contributes the leading effect to the dynamics and equilibrium of the droplet. Especially, for the contact line  $\Gamma$ , where three phases of materials (gas, liquid, and solid) meet, one should consider the interactions between their surface energy. Denote  $\gamma_{sl} > 0$  ( $\gamma_{sg}, \gamma_{lg}$  resp.) as the interfacial surface energy density (a.k.a. surface tension coefficients) between solid-liquid phases (solid-gas, liquid-gas resp.). To measure the total area of the capillary surface with surface tension  $\gamma_{lg}$  and the area of the contact domain with the relative surface tension  $\gamma_{sl} - \gamma_{sg}$ , we take the total free energy of the droplet as the summation of surface energy and gravitational energy

$$(3.6) \quad \begin{aligned} \mathcal{F} &= \gamma_{lg} \int_{\partial A(t) \cap \{u > 0\}} \, ds + (\gamma_{sl} - \gamma_{sg}) \int_{D(t)} \, dx \, dy + \rho g \int_{D(t)} \frac{u^2}{2} \, dx \, dy, \\ &= \gamma_{lg} \int_{D(t)} \sqrt{1 + |\nabla u|^2} \, dx \, dy + (\gamma_{sl} - \gamma_{sg}) \int_{D(t)} \, dx \, dy + \rho g \int_{D(t)} \frac{u^2}{2} \, dx \, dy, \end{aligned}$$

where  $\rho$  is the density of the liquid,  $g$  is the gravitational acceleration. Besides gravity, we neglect other forces, such as inertia effect, viscosity stress inside the droplet, Marangoni effect, electromagnetic fields, evaporation and condensation, etc.

With a fixed volume  $V$ , the competition between the three surface tension coefficients will determine uniquely the steady state of the droplet, i.e. the minimizer of  $\mathcal{F}$ . By Young's equation [38], the equilibrium contact angle  $\theta_Y$  is determined by the Young's angle condition

$$(3.7) \quad \cos \theta_Y = \frac{\gamma_{sg} - \gamma_{sl}}{\gamma_{lg}}.$$

Denote relative adhesion coefficient between the liquid and the solid as

$$\sigma := \frac{\gamma_{sl} - \gamma_{sg}}{\gamma_{lg}} = -\cos \theta_Y.$$

We will focus on the partially wetting (hydrophilic) case  $-1 < \sigma < 0$ , or equivalently  $0 < \theta_Y < \frac{\pi}{2}$ . In this case, adhesive forces between the liquid and the solid tend to spread the droplet across the surface and there is a vertical graph representation of the capillary surface. We refer to [16] for

more discussions on dewetting or non-wetting droplets (i.e.  $0 < \sigma < 1$ ) with a horizontal graph representation for quasi-static case.

**3.1.3. Viscosity damping force for the motion of droplet and Rayleigh dissipation function.** If we neglect the viscosity stress inside the droplet, there are two types of viscosity damping force on the droplet. First, the contact line friction force density is given by  $-\mathcal{R}v_{cl}n_{cl} = -\mathcal{R}(n_{cl} \cdot \nabla_{x,y}\phi)n_{cl}$ , where  $\mathcal{R}$  is the viscosity damping coefficient per unit length for the contact line with the units of mass/(length · time). Second, the viscosity damping friction force density on the capillary surface is given by  $-\zeta v_n n$ , where  $\zeta$  is the viscosity damping coefficient per unit area for the capillary surface with the units of mass/(area · time). Then the Rayleigh dissipation function (in the unit of work) is given by [18]

$$(3.8) \quad Q = \frac{\mathcal{R}}{2} \int_{\Gamma(t)} |v_{cl}|^2 \, ds + \frac{\zeta}{2} \int_{\partial A(t) \cap \{u > 0\}} |v_n|^2 \, ds.$$

With the driven energy (3.6) and Rayleigh's dissipation function (3.8), the motion of the droplets can be completely described by the geometric configurations: the contact line  $\Gamma(t)$ , capillary surface  $u(x, y, t)$  and their speed.

**3.2. Dynamics of a droplet with topological changes as a gradient flow on manifold.** With the specific driven energy  $\mathcal{F}$  on manifold  $\mathcal{M}$  and dissipation function (3.8), we now start to model the droplets dynamics using gradient flow on manifold  $\mathcal{M}$  described below.

Here we first give the derivation by taking rough impermeable substrate as  $z = 0$  for simplicity. We use a Hilbert manifold [28] to describe the configuration space

$$(3.9) \quad \mathcal{M} := \{(\Gamma, u); \Gamma := \partial D \in C^1, u \in H_0^1(D), u \geq 0 \text{ on } D\}.$$

The dynamics of the droplet is represented by a trajectory on this manifold. Consider a trajectory  $\eta(t) \in \mathcal{M}$  starting from initial state  $\eta(0) = \{\Gamma(0), u(x, y, 0)\} \in \mathcal{M}$ ,

$$(3.10) \quad \eta(t) = \{\Gamma(t), u(x, y, t)\} \in \mathcal{M}, \quad t \in [0, T].$$

Now we use the vertical velocity  $v = \partial_t u$  and the contact line velocity  $\partial_t \Gamma = v_{cl}n_{cl}$  to describe the tangent plane  $T_\eta \mathcal{M}$ . Since the geometric motion has an obstacle condition  $u \geq 0$ , manifold  $\mathcal{M}$  has a boundary, i.e.  $\{\eta \in \mathcal{M}; u(x, y) = 0 \text{ for some } (x, y) \in D\}$ . This will lead to an EVI/PVI as described below when the droplet has a splitting. On the boundary, the tangent plane is not a linear space and has the restriction

$$(3.11) \quad \begin{aligned} \frac{du(\Gamma(t), t)}{dt} &= \partial_t u(\Gamma(t), t) + \nabla u(\Gamma(t), t) \cdot \partial_t \Gamma \\ &= \partial_t u(\Gamma(t), t) + (\nabla u(\Gamma(t), t) \cdot n_{cl})v_{cl} \\ &= \partial_t u(\Gamma(t), t) - |\nabla u(\Gamma(t), t)|v_{cl} = 0, \end{aligned}$$

where we used the fact that  $\nabla u(\Gamma(t), t) \cdot n_{cl} = -|\nabla u(\Gamma(t), t)|$  in the graph representation. The tangent plane at  $\eta$  is given by

$$(3.12) \quad T_\eta \mathcal{M} := \{(v_{cl}, v); \partial_t u(\Gamma(t), t) - |\nabla u(\Gamma(t), t)|v_{cl} = 0, v + u \geq 0 \text{ in } D(t)\}.$$

The last inequality for  $T_\eta \mathcal{M}$  in (3.12) becomes effective when  $\eta$  sits on the boundary of the manifold  $\mathcal{M}$ , i.e.  $u = 0, v \geq 0$  when  $u$  touches the impermeable obstacle. Define the contact angles (inside the droplet  $A$  in Fig 1 (a)) as

$$(3.13) \quad \tan \theta_{cl} := |\nabla u(\Gamma)|.$$

Then (3.12) reflects the natural physical meaning of contact angle

$$(3.14) \quad \tan \theta_{cl} = |\nabla u(\Gamma)| = \frac{\partial_t u|_\Gamma}{v_{cl}},$$

i.e. the dynamic contact angle is always determined by the quotient of the vertical velocity and the horizontal velocity. Notice the outer normal  $n = \frac{1}{1+|\nabla u|^2}(-\nabla u, 1)$  on the capillary surface and due to  $\lim_{z \rightarrow 0^+} -\nabla u = |\nabla u|n_{cl}$ ,  $\lim_{z \rightarrow 0^+} n = \frac{1}{1+|\nabla u|^2}(|\nabla u|n_{cl}, 1)$ . Using the contact angle  $\theta_{cl}$ , we have

$$(3.15) \quad \lim_{z \rightarrow 0^+} n = (\sin \theta_{cl} n_{cl}, \cos \theta_{cl}), \quad \lim_{z \rightarrow 0^+} v_n = \sin \theta_{cl} v_{cl}.$$

Next, we describe the dissipation mechanism of the dynamics. From Rayleigh's dissipation function (3.8), which gives the rate of energy dissipation  $2Q$  due to friction[18], it is natural to introduce the Riemannian metric  $g_\eta$  on  $T_\eta \mathcal{M} \times T_\eta \mathcal{M}$  as

$$(3.16) \quad g_\eta(q_1, q_2) := \mathcal{R} \int_{\Gamma(t)} v_{cl1} v_{cl2} \, ds + \zeta \int_{D(t)} v_1 v_2 \frac{dx \, dy}{\sqrt{1 + |\nabla u|^2}}$$

for any  $q_1 = (v_{cl1}, v_1), q_2 = (v_{cl2}, v_2) \in T_\eta \mathcal{M}$ ; see also DAVIS [10], [29], DOI [37] and [19].

We are now in the position to derive the gradient flow of  $\mathcal{F}(\eta)$  on manifold  $\mathcal{M}$  with respect to the Riemannian metric  $g_\eta$ . For an arbitrary trajectory  $\tilde{\eta}(s) = \{\tilde{\Gamma}(s), \tilde{u}(x, y, s)\}$  (a.k.a. virtual displacement) starting from  $\tilde{\eta}(t) = \eta(t)$  at the tangent direction

$$(3.17) \quad \tilde{\eta}'(t) = \{\partial_t \tilde{\Gamma}(t), \partial_t \tilde{u}\} = \{\tilde{v}_{cl}, \tilde{v}\} \in T_{\eta(t)} \mathcal{M},$$

we know

$$(3.18) \quad \tilde{v}|_\Gamma = |\nabla u(\Gamma(t), t)| \tilde{v}_{cl}.$$

To ensure the volume preserving condition  $\int_{D(t)} u \, dx \, dy = V$ ,  $t \in [0, T]$ , we consider the gradient flow of extended free energy  $\mathcal{F}(\eta, \lambda)$  on manifold  $\mathcal{M} \times \mathbb{R}$  for  $\eta(t) \in \mathcal{M}$  and a Lagrange multiplier  $\lambda(t)$

$$(3.19) \quad \mathcal{F}(\eta(t), \lambda(t)) = \mathcal{F}(\eta(t)) - \lambda(t) \left( \int_{D(t)} u(t) \, dx \, dy - V \right).$$

Since the Lagrange multiplier  $\lambda(t)$  does not bring any dissipation into the dynamics, we only give the derivation of the gradient flow on  $\mathcal{M}$  for simplicity.

We regard the Riemannian manifold  $\mathcal{M}$  as a metric space with the distance  $\text{dist}(\cdot, \cdot)$  induced by the length of geodesic. Following [2, Theorem 4.0.13], the EVI for gradient flow on  $\mathcal{M}$  is

$$(3.20) \quad \frac{1}{2} \frac{d}{dt} \text{dist}(\eta(t), v)^2 \leq \mathcal{F}(v) - \mathcal{F}(\eta(t)), \quad \text{for a.e. } t > 0, \forall v \in \mathcal{M}.$$

From [33, P 633], for any  $v \in \exp_{\eta(t)}(\varepsilon \tilde{\eta}')$ , i.e., the exponential map with initial tangent vector  $\varepsilon \tilde{\eta}' \in T_{\eta(t)} \mathcal{M}$  and  $\varepsilon > 0$  small enough such that there exists a unique geodesic  $\Upsilon$  connecting  $\eta(t)$

to  $v$ , we have

$$(3.21) \quad \frac{1}{2} \frac{d}{dt} \text{dist}(\eta(t), v)^2 = -g_{\eta(t)}(\varepsilon \tilde{\eta}'(t), \eta'(t)),$$

where Riemannian metric  $g_\eta$  defined in (3.16). Then when  $\mathcal{F}$  is directionally differentiable, i.e.  $\mathcal{F} \circ \Upsilon_\tau$  is differentiable at  $\tau = 0^+$  for any geodesics  $\Upsilon_\tau$  starting from  $\eta(t)$ , by (3.21) and [33, Proposition 23.1 (iv)],

$$(3.22) \quad -g_{\eta(t)}(\varepsilon \tilde{\eta}'(t), \eta'(t)) = \frac{1}{2} \frac{d}{dt} \text{dist}(\eta(t), \exp_{\eta(t)}(\varepsilon \tilde{\eta}'))^2 \leq \lim_{\tau \rightarrow 0^+} \frac{\mathcal{F}(\exp_{\eta(t)}(\tau \varepsilon \tilde{\eta}')) - \mathcal{F}(\eta(t))}{\tau}.$$

Therefore for any  $\tilde{\eta}'(t) \in T_{\eta(t)}\mathcal{M}$ , any  $\tilde{\lambda}'(t) \in \mathbb{R}$  and geodesics

$$(3.23) \quad \tilde{\eta}(s) = \exp_{\eta(t)}((s-t)\tilde{\eta}'(t)) \in \mathcal{M}, \quad \tilde{\lambda}(s) = \exp_{\lambda(t)}((s-t)\tilde{\lambda}'(t)) \in \mathbb{R},$$

the gradient flow of  $\mathcal{F}(\eta, \lambda)$  with respect to Riemannian metric  $g_\eta$  defined in (3.16) becomes

$$(3.24) \quad \begin{aligned} -g_{\eta(t)}(\tilde{\eta}'(t), \eta'(t)) &\leq \frac{d}{ds} \Big|_{s=t^+} \mathcal{F}(\tilde{\eta}(s), \tilde{\lambda}(s)) \\ &= \frac{d}{ds} \Big|_{s=t^+} \mathcal{F}(\tilde{\eta}(t)) - \frac{d}{ds} \Big|_{s=t^+} \tilde{\lambda}(s) \left( \int_{\tilde{D}(s)} \tilde{u}(s) dx dy - V \right) \\ &= \frac{d}{ds} \Big|_{s=t^+} \mathcal{F}(\tilde{\eta}(s)) - \lambda(t) \int_{D(t)} \tilde{v}(t) dx dy - \tilde{\lambda}'(t) \left( \int_{D(t)} u dx dy - V \right), \end{aligned}$$

where we used (3.17) and the Reynolds transport (3.5) in the last equality. For a generic free energy density  $G(u, \nabla u)$ , we calculate the first variation  $\frac{d}{ds} \Big|_{s=t^+} \int_{\tilde{D}(t)} G(\tilde{u}(x, y, s), \nabla \tilde{u}(x, y, s)) dx dy$  below. Three typical free energy examples included in this setup are: (i) Dirichlet energy  $G(u, \nabla u) = \frac{1}{2} |\nabla u|^2 + \sigma$ , c.f. [5, 22, 14, 37]; (ii) Area functional  $G(u, \nabla u) = \sqrt{1 + |\nabla u|^2} + \sigma$ , c.f. [6, 7, 15]; (iii) free energy for droplets on inclined groove-textured surface; see (3.30) below.

From (3.18) and the Reynolds transport theorem,

$$(3.25) \quad \begin{aligned} &\frac{d}{ds} \Big|_{s=t^+} \int_{\tilde{D}(t)} G(\tilde{u}(x, y, s), \nabla \tilde{u}(x, y, s)) dx dy \\ &= \int_{\Gamma(t)} G|_\Gamma \tilde{v}_{cl} ds + \int_{D(t)} \partial_u G \tilde{v} + \partial_{\nabla u} G \cdot \nabla \tilde{v} dx dy \\ &= \int_{\Gamma(t)} G|_\Gamma \tilde{v}_{cl} ds + \int_{D(t)} (\partial_u G - \nabla \cdot (\partial_{\nabla u} G)) \tilde{v} dx dy + \int_{\Gamma(t)} \tilde{v} (n_{cl} \cdot \partial_{\nabla u} G) ds \\ &= \int_{\Gamma} [G + |\nabla u| (n_{cl} \cdot \partial_{\nabla u} G)] \Big|_{\Gamma} \tilde{v}_{cl} ds + \int_{D(t)} (\partial_u G - \nabla \cdot (\partial_{\nabla u} G)) \tilde{v} dx dy. \end{aligned}$$

Notice from  $\tilde{\eta}(t) = \eta(t)$ , the Riemannian metric  $g_{\eta(t)}$ ,

$$(3.26) \quad g_\eta(\tilde{\eta}(t), \eta(t)) := \mathcal{R} \int_{\Gamma(t)} \tilde{v}_{cl} v_{cl} ds + \zeta \int_{D(t)} \tilde{v} \frac{\partial_t u}{\sqrt{1 + |\nabla u|^2}} dx dy.$$

where  $\frac{\partial_t u(x, t)}{\sqrt{1 + (\partial_x u)^2}}$  is the normal velocity in the direction of the outer normal. Hence by taking different  $\tilde{\eta}' \in T_{\eta(t)}\mathcal{M}$  and arbitrary  $\tilde{\lambda}' \in \mathbb{R}$ , the governing equations for  $u(\cdot, t) \in H_0^1(D(t))$  and  $\lambda(t)$

are

$$\begin{aligned}
(3.27) \quad & \mathcal{R}v_{cl} = -[G + |\nabla u|(n_{cl} \cdot \partial_{\nabla u} G)]|_{\Gamma}, \\
& \int_{D(t)} \left[ \zeta \frac{\partial_t u}{\sqrt{1 + |\nabla u|^2}} + (\partial_u G - \nabla \cdot (\partial_{\nabla u} G)) - \lambda(t) \right] v \, dx \, dy \geq 0, \\
& \forall v \in H_0^1(D(t)), v(x) + u(x, t) \geq 0, \\
& \int_{D(t)} u \, dx \, dy = V
\end{aligned}$$

with initial data  $\eta(0) = \{\Gamma(0), u(x, y, 0)\}$  and initial volume  $V$ .

The parabolic variational inequality (PVI) above is able to describe the merging and splitting of several drops. However, whenever topological changes happen, (3.27) can not describe the correct phase transition at the splitting/merging point. For instance, when one droplet splits into two droplets, physically, at the splitting domain  $D_0 := \{(x, y) \in \text{int}D; u(x, t) = 0\}$ , the interface between gas and liquid becomes the interface between gas and solid, therefore new contact lines with competitions from three phases appear. Instead, the dynamics governing by PVI (3.27) does not contain these phase transition information but only leads to nonphysical motion at the splitting domain  $D_0$ , i.e. droplet is allowed to move along the boundary  $D_0$ . We propose the following natural method to incorporate the phase transition information into dynamics after splitting. (I) We first detect when and where the phase transition happens by recording the new generated contact lines. (II) Then surface energies from three phases take over the dynamics posterior to splitting. That is to say, the generated two droplets have the same governing equation with (3.27) respectively and the volume of each droplet is preserving over time. See the detailed algorithm in Section 4.1

**3.2.1. Gradient flow formulation of a droplet placed on a groove-textured and inclined surface with splitting.** In this section, we focus on a 2D droplet placed on a groove-textured and inclined surface and use the PVI obtained in (3.27) to derive the governing PVI. Given a groove-textured impermeable surface described by a graph function  $w(x)$ , a droplet is then described by

$$(3.28) \quad A := \{(x, y); a \leq x \leq b, w(x) \leq y \leq u(x) + w(x)\}.$$

Following the convention, we use the Cartesian coordinate system built on an inclined plane with effective inclined angle  $\theta_0$  such that  $-\frac{\pi}{2} < \theta_0 < \frac{\pi}{2}$  and  $(\tan \theta_0)x$  is the new  $x$ -axis. Denote the height function as

$$h(x, t) := u(x, t) + w(x).$$

To be consistent with the height function  $u$  in the last section, we choose the configuration states of this droplet as the relative height function (capillary surface)  $u(x, t) \geq 0$  and partially wetting domain  $a(t) \leq x \leq b(t)$  with free boundaries  $a(t), b(t)$ . Consider the manifold

$$(3.29) \quad \mathcal{M} := \{a, b, u(x); u(x) \geq 0, u(x) \in H_0^1(a, b)\}.$$

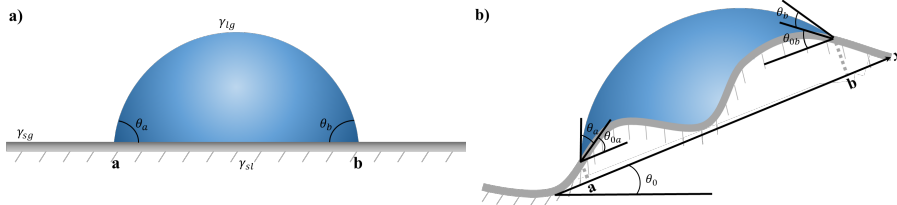


FIGURE 1. Droplets with contact angles  $\theta_a, \theta_b$ . (a) Droplet placed on  $z = 0$ ; (b) Droplet placed on inclined groove-textured surface with effective angle  $\theta_0$ .

Consider the energy functional associated with the groove-textured surface

$$(3.30) \quad \begin{aligned} \mathcal{F}(\eta(t)) = & \gamma_{lg} \int_{a(t)}^{b(t)} \sqrt{1 + (\partial_x(u + w))^2} dx + (\gamma_{sl} - \gamma_{sg}) \int_{a(t)}^{b(t)} \sqrt{1 + (\partial_x w)^2} dx \\ & + \rho g \int_{a(t)}^{b(t)} \int_{h_0}^{u+h_0} (y \cos \theta_0 + x \sin \theta_0) dy dx, \end{aligned}$$

where  $\rho$  is the density of the liquid,  $g$  is the gravitational acceleration. Then we have

$$(3.31) \quad \begin{aligned} G(u, x) = & \sqrt{1 + (\partial_x(u + w))^2} + \sigma \sqrt{1 + (\partial_x w)^2} + \frac{\rho g}{\gamma_{lg}} \left( \frac{u^2 \cos \theta_0}{2} + \cos \theta_0 uw + x \sin \theta_0 u \right) \\ \partial_u G = & \frac{\rho g}{\gamma_{lg}} ((u + w) \cos \theta_0 + x \sin \theta_0), \quad \partial_{u_x} G = \frac{\partial_x(u + w)}{\sqrt{1 + (\partial_x(u + w))^2}}. \end{aligned}$$

Define the tangential plane at  $\eta$  as

$$(3.32) \quad T_\eta \mathcal{M} := \{a', b', v(x) \in H^1(a, b); v(x) + u(x) \geq 0, v(a) = -\partial_x u(a)a', v(b) = -\partial_x u(b)b'\}$$

associated with the Riemannian metric  $g_{\eta(t)} : T_{\eta(t)} \mathcal{M} \times T_{\eta(t)} \mathcal{M} \rightarrow \mathbb{R}$

$$(3.33) \quad g_{\eta(t)}(\tilde{\eta}'(t), \eta'(t)) = \mathcal{R} \tilde{a}' a'(t) + \mathcal{R} \tilde{b}' b'(t) + \zeta \int_{a(t)}^{b(t)} \tilde{v} \frac{\partial_t u(x, t)}{\sqrt{1 + (\partial_x(u + w))^2}} dx,$$

where  $\tilde{\eta}' = (\tilde{a}', \tilde{b}', \tilde{v}(x))$  and  $\frac{\partial_t u(x, t)}{\sqrt{1 + (\partial_x(u + w))^2}}$  is the normal velocity along the outer normal direction.

*Remark 1.* Let the density of gas outside the droplet is  $\rho_0 = 0$ . We denote the capillary coefficient as  $\varsigma := \frac{\rho g}{\gamma_{lg}} > 0$  and the capillary length as  $L_c := \frac{1}{\sqrt{\varsigma}}$ . For a droplet with volume  $V$ , its equivalent length (characteristic length)  $L$  is defined as  $V = \frac{4\pi}{3} L^3$  in 3D and  $V = \pi L^2$  in 2D. The Bond number  $Bo := (\frac{L}{L_c})^2 = \varsigma L^2$  shall be small enough to observe the capillary effect [11]. In the inclined case, for a droplet with volume  $V$  in 2D, the effective Bond number is  $Bo := \left(\frac{L}{L_c}\right)^2 \cos \theta_0 = \varsigma L^2 \cos \theta_0$ . After dimensionless argument, we use the new dimensionless constant  $\beta, \kappa$  in the governing equation below.

Then (3.27) gives the governing PVI<sup>1</sup> for the 2D droplet

$$\begin{aligned}
 & \int_{a(t)}^{b(t)} \left( \beta \frac{\partial_t h(x, t)}{\sqrt{1 + (\partial_x h)^2}} - \frac{\partial}{\partial x} \left( \frac{\partial_x h}{\sqrt{1 + (\partial_x h)^2}} \right) + \kappa(h \cos \theta_0 + x \sin \theta_0) - \lambda(t) \right) v \, dx \geq 0, \\
 & \quad \text{for any } v(x) \in H^1(a, b); \quad v(x) + u(x) \geq 0, \\
 & \quad u(a(t), t) = u(b(t), t) = 0, \\
 (3.34) \quad a'(t) &= \sigma \sqrt{1 + (\partial_x w)^2} + \frac{1 + \partial_x h \partial_x w}{\sqrt{1 + (\partial_x h)^2}} = \frac{1}{\cos \theta_{0a}} (\cos \theta_a - \cos \theta_Y), \quad x = a(t), \\
 b'(t) &= -\sigma \sqrt{1 + (\partial_x w)^2} - \frac{1 + \partial_x h \partial_x w}{\sqrt{1 + (\partial_x h)^2}} = -\frac{1}{\cos \theta_{0b}} (\cos \theta_b - \cos \theta_Y), \quad x = b(t), \\
 & \quad \int_{a(t)}^{b(t)} u(x, t) \, dx = V,
 \end{aligned}$$

where  $\theta_a, \theta_b$  are two contact angles at  $a(t), b(t)$  and  $\partial_x w|_a = \tan \theta_{0a}, \partial_x h|_a = \tan(\theta_{0a} + \theta_a)$  and  $\partial_x w|_b = -\tan \theta_{0b}$  and  $\partial_x h|_b = -\tan(\theta_{0b} + \theta_b)$ ; see Fig 1 (b). It is easy to check the steady state  $a'(t) = b'(t) = 0$  recovers Young's angle condition.

#### 4. NUMERICAL SCHEMES AND SIMULATIONS

**4.1. Proposed numerical schemes based on explicit boundary moving and projection method.** In this section, we propose numerical schemes for droplets dynamics with merging and splitting, which is an extension of the 1st/2nd order schemes developed in [16] for single droplet without topological changes. To incorporate the splitting due to an impermeable obstacle, we need to solve the PVI (3.34) instead of PDEs. Inspired by the Trotter-Kato's product formula (2.9) in Section 2, instead of solving PVI (3.34), we adapt the projection method discussed in Section 2 to solve PVI (3.34). More precisely, we solve gradient flow equality and projection to  $\mathcal{M}$  iteratively at each time step; see detailed below. Although the stability and convergence theory developed in Section 2 is only for PVI in Hilbert space, the method can be used to solve gradient flows on Hilbert manifold in PVI formulation. The convergence analysis for the projection method in Hilbert manifold setting is indeed hard, but we focus on the algorithms and numerical experiments in this section. First, we further split the gradient flow equality solver into two steps: (i) explicit boundary updates and (ii) semi-implicit capillary surface updates. The unconditional stability for explicit 1D boundary updates is proved in [16], which efficiently decouples the computations of the boundary evolution and the capillary surface updates. The semi-implicit capillary surface updates without obstacle but with volume constraint can be convert to a standard elliptic solver at each step. Next, to enforce the impermeable obstacle, we (iii) project the capillary surface to the manifold  $\mathcal{M}$ . This step has explicit formula so also keeps the efficiency. Finally, to incorporate the phase transition information explained in Section 3.2, we (iv) detect the splitting point after some threshold and add new contact line updates after that.

*First order scheme for splitting:*

Step 1. Explicit boundary updates. Compute the one-side approximated derivative of  $h^n$  at  $b^n$  and  $a^n$ , denoted as  $(\partial_x h^n)_N$  and  $(\partial_x h^n)_0$ . Then by the dynamic boundary condition in (3.34), we

<sup>1</sup>By changing variable  $\tilde{v} := v + u$  in the first inequality, then it is the standard formulation of PVI.

update  $a^{n+1}, b^{n+1}$  using

$$(4.1) \quad \begin{aligned} \frac{a^{n+1} - a^n}{\Delta t} &= \sigma \sqrt{1 + (\partial_x w)_0^2} + \frac{1 + (\partial_x h^n)_0 (\partial_x w)_0}{\sqrt{1 + (\partial_x h^n)_0^2}}, \\ \frac{b^{n+1} - b^n}{\Delta t} &= -\sigma \sqrt{1 + (\partial_x w)_N^2} - \frac{1 + (\partial_x h^n)_N (\partial_x w)_N}{\sqrt{1 + (\partial_x h^n)_N^2}}. \end{aligned}$$

Step 2. Rescale  $h^n$  from  $[a^n, b^n]$  to  $[a^{n+1}, b^{n+1}]$  with  $O(\Delta t^2)$  accuracy using a semi-Lagrangian discretization. For  $x^{n+1} \in [a^{n+1}, b^{n+1}]$ , denote the map from moving grids at  $t^{n+1}$  to  $t^n$  as

$$(4.2) \quad x^n := a^n + \frac{b^n - a^n}{b^{n+1} - a^{n+1}} (x^{n+1} - a^{n+1}) \in [a^n, b^n].$$

Define the rescaled solution for  $h^n$  as

$$(4.3) \quad h^{n*}(x^{n+1}) := h^n(x^n) + \partial_x h^n(x^n)(x^{n+1} - x^n).$$

It is easy to verify by the Taylor expansion  $h^{n*}(x^{n+1}) = h^n(x^{n+1}) + O(|x^n - x^{n+1}|^2)$ .

Step 3. Capillary surface updates without impermeable obstacle constraint, but with volume revising constraint. Update  $\tilde{h}^{n+1}$  and  $\lambda^{n+1}$  semi-implicitly.

$$(4.4) \quad \begin{aligned} \frac{\beta}{\sqrt{1 + (\partial_x h^{n*})^2}} \frac{\tilde{h}^{n+1} - h^{n*}}{\Delta t} &= \frac{\partial}{\partial x} \left( \frac{\partial_x \tilde{h}^{n+1}}{\sqrt{1 + (\partial_x h^{n*})^2}} \right) - \kappa(h^{n+1} \cos \theta_0 + x^{n+1} \sin \theta_0) + \lambda^{n+1}, \\ \tilde{h}^{n+1}(a^{n+1}) &= w(a^{n+1}), \quad \tilde{h}^{n+1}(b^{n+1}) = w(b^{n+1}), \\ \int_{a^{n+1}}^{b^{n+1}} \tilde{u}^{n+1}(x^{n+1}) \, dx^{n+1} &= \int_{a^0}^{b^0} u^0(x^0) \, dx^0, \end{aligned}$$

where the independent variable is  $x^{n+1} \in (a^{n+1}, b^{n+1})$ .

Step 4. Enforce impermeable obstacle condition by projection. If  $\tilde{h}^{n+1} < w$  for some  $D_0 := (c^{n+1}, d^{n+1}) \subset (a^{n+1}, b^{n+1})$  project to manifold  $\mathcal{M}$

$$(4.5) \quad h^{n+1} = \text{Proj}_{\mathcal{M}}(\tilde{h}^{n+1}) = \max\{\tilde{h}^{n+1}, w\}.$$

Step 5. Detect phase transition. Let  $\varepsilon > 0$  be a threshold parameter. If the length of splitting domain  $D_0 > \varepsilon$ , then record two new endpoints  $c^{n+1}, d^{n+1}$  and regard the current profile  $h^{n+1}$  on  $(a^{n+1}, c^{n+1})$  and  $(d^{n+1}, b^{n+1})$  as two independent droplets and the total volume of these two droplet remains same.

*First order scheme for merging:* The numerical scheme for the dynamics of two independent droplets with endpoints  $a_1^n, b_1^n$  ( $a_2^n, b_2^n$  resp.) are same as Step 1-3. To detect the merging of two independent droplets, at each time stepping  $t^n$ , one also need a threshold parameter  $\varepsilon > 0$  such that we treat two droplets as one big droplet if  $|a_2^n - b_1^n| < \varepsilon$ .

The projection method for droplets dynamics above also works for second order scheme, which replaces Step 1-3 by middle-point schemes. We omit details and refer to [16].

*Remark 2.* Notice for the splitting case, the projection (Step 4) will lose a little volume. However, the volume constraint in the iteration Step 3 will maintain the total volume of the droplet upto machine accuracy. In the splitting step (Step 5), we also enforce the total volume remains same. Notice also we work on moving grids associated with the moving boundaries, so splitting step does not introduce spacial local error.

TABLE 1. Ten points used in Bézier curve fitting of geometry of the Utah teapot

$i$	1	2	3	4	5	6	7	8	9	10
$x_i$	-2	$-\frac{4}{3}$	$-\frac{2}{3}$	0	$\frac{2}{3}$	$\frac{4}{3}$	2	2.655	2.846	4
$y_i$	0.78	0	0	0	0	0	0.78	1.142	2.146	2.5

**4.2. Simulations for merging and splitting of droplets.** In this section, we demonstrate two typical examples using the projection scheme in Section 4.1. The first example is the splitting of one big droplet into two droplets when placed on an inclined groove-textured substrate. The second example is the merging of two droplets in Utah teapot, which is compared to the independent dynamics of two droplets in teapot separately.

Example 1: Splitting of one droplet on an inclined groove-textured substrate. We take a typical groove-textured substrate

$$(4.6) \quad w(x) = A(\sin(kx) + \cos(2kx))^2, \quad A = 0.1, \quad k = 2.5.$$

This is an impermeable obstacle where phase transitions happen when the droplet touches the obstacle. Thus at the touching point, after one detect the phase transition, one droplet will split into two independent droplets with their own PVI (3.34). To demonstrate those phenomena, we take the physical parameters as  $\kappa = 1$ ,  $\beta = 0.1$ , effective inclined angle  $\theta_0 = 0.3$  and initial droplet as

$$(4.7) \quad h(x, 0) = 0.1(x - a(0))(b(0) - x) + w(a(0)) + \frac{[w(b(0)) - w(a(0))](x - a(0))}{b(0) - a(0)}$$

with initial endpoints  $a(0) = -2.1$ ,  $b(0) = 3.1$  as shown in Fig 2 using green line. The corresponding effective Bond number can be calculated as Remark 1 with effective inclined angle  $\theta_0 = 0.3$ ,  $Bo = 0.5712$ . We take final time as  $T = 1$  with time step  $\Delta t = 0.005$  and use  $N = 200$  moving grids uniformly in  $(a(t), b(t))$  in the projection scheme. With relative adhesion coefficient  $\sigma = -0.52$ , in Fig. 2, we show the dynamics of the droplet on groove-textured surface  $w(x)$  in (4.6) at equal time intervals using thin red lines. The splitting time detected is  $T_s = 0.035$  with threshold  $\varepsilon = 0.075$  and the two generated droplets keep moving independently until the final time  $T = 1$  with the final profiles shown in solid blue lines.

Example 2: Two droplets merged together in the Utah teapot.

We use the Utah teapot, which is well-known in computer graphics history, as a typical inclined groove-textured substrate to demonstrate the merging of two droplets. The Utah teapot can be constructed by several cubic Bézier curves [3] connecting the following ten points  $x_i, y_i$ ,  $i = 1, \dots, 10$  as listed in Table 1. For the bottom of the teapot, we use  $(x_i, y_i)$  for  $i = 1, \dots, 4$  and  $(x_i, y_i)$  for  $i = 4, \dots, 7$ . For the mouth of the teapot, we use  $(x_i, y_i)$  for  $i = 7, \dots, 10$ . Assume the inclined groove-textured substrate is expressed by parametric curve  $(x(\ell), y(\ell))$ . Let  $\ell(x)$  be the inverse function of  $x(\ell)$ , then  $w(x) = y(\ell(x))$  in (3.34).

Now we take the physical parameters as  $\kappa = 20$ ,  $\beta = 1$  and the relative adhesion coefficient as  $\sigma = -0.78$ . Assume the initial droplet 1 is

$$(4.8) \quad h(x, 0) = 4.5(x - a(0))(b(0) - x) + w(a(0)) + \frac{[w(b(0)) - w(a(0))](x - a(0))}{b(0) - a(0)}$$

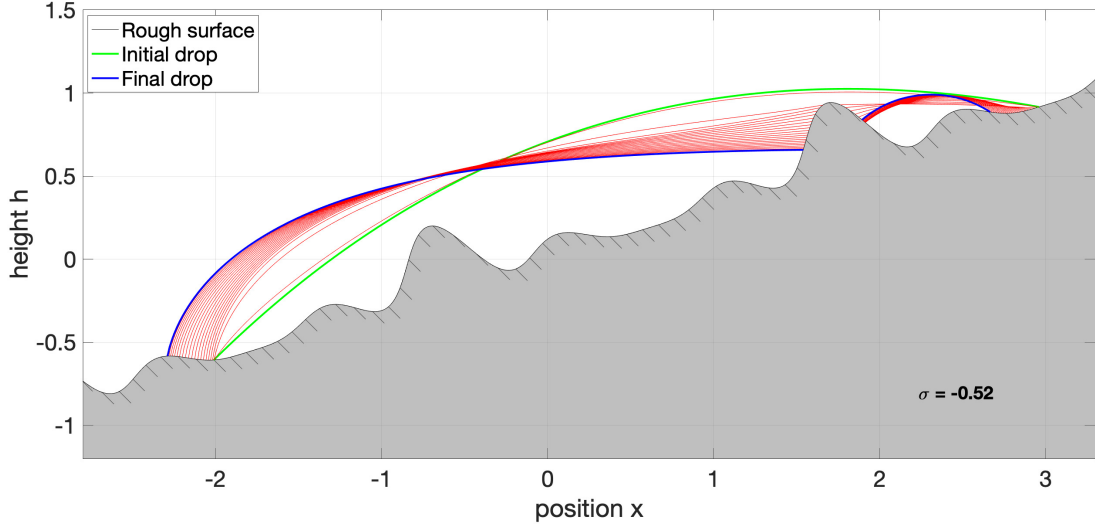


FIGURE 2. Evolution and splitting of one droplet into two droplets on inclined groove-textured surfaces using the projection scheme in Section 4.1. Parameters:  $\kappa = 1$ ,  $\beta = 0.1$ , number of moving grids in drop  $N = 200$ , time step  $\Delta t = 0.005$ , final time  $T = 1$ , splitting threshold  $\varepsilon = 0.075$ , initial drop profile (green line)  $h(x, t)$  in (4.7) with initial endpoints  $a(0) = -2.1, b(0) = 3.1$ , Bond number  $Bo = 0.5712$ , relative adhesion coefficient  $\sigma = -0.95$  and inclined substrate with effective angle  $\theta_0 = 0.3$  and (4.6). The evolution is shown using red line at equal time intervals and the final profiles of two new droplets are shown in blue line.

with initial endpoints  $a(0) = 1.9, b(0) = 2.2$ ; as shown in Fig 3 with magenta double-dotted line. Assume the initial droplet 2 as

$$(4.9) \quad h(x, 0) = 7.8(x - a(0))(b(0) - x) + w(a(0)) + \frac{[w(b(0)) - w(a(0))](x - a(0))}{b(0) - a(0)}$$

with initial endpoints  $a(0) = 2.4, b(0) = 2.9$  as shown in Fig 3 with green double-dotted line. The corresponding effective Bond number can be calculated according to Remark 1 with effective inclined angle  $\theta_0 = 0.226\pi$ ,  $Bo = 0.0832$  for Droplet 1 while  $Bo = 0.7861$  for Droplet 2. In the numeric scheme, we use  $N = 1000$  moving grids uniformly in  $(a(t), b(t))$  and the merging threshold  $\varepsilon = 0.01$ . We take the same final time  $T = 12$  with time step  $\Delta t = 0.05$ . Without merging, the dynamics at equal time intervals of Droplet 1 and Droplet 2 are shown separately as comparisons in Fig 3 (upper/middle) with the final profile at  $T = 12$  using solid magenta line for Droplet 1 and solid green line for Droplet 2. The small magenta Droplet 1 (upper) shows slow capillary rise, while the large green Droplet 2 (middle) moves down fast due to gravitational effect. However, with the same parameters and same initial profiles (double-dotted lines), the dynamics at equal time intervals for the two droplets placed together in the Utah teapot are shown in Fig 3 (down). The two droplets will merge together at  $T = 3$  with the solid magenta/green lines for Droplet 1/Droplet 2 and then they continue to move down as a new big droplet as shown in thin blue lines. The final profile of the new big droplet at  $T = 12$  is shown in solid blue line.

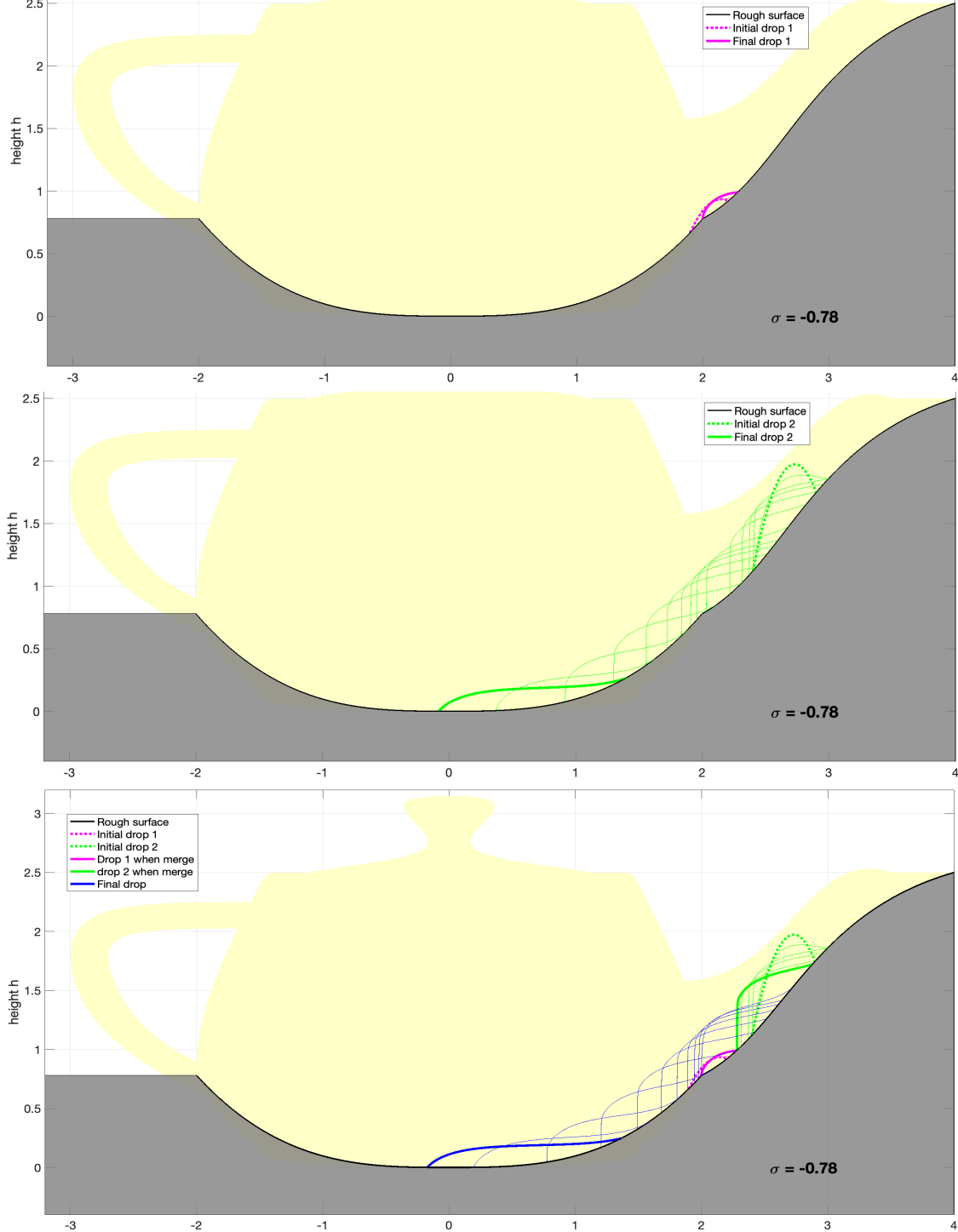


FIGURE 3. Evolution of two partially wetting droplets in the Utah teapot at equal time intervals using the scheme in Section 4.1. Parameters: number of moving grids in drop  $N = 1000$ , time step  $\Delta t = 0.05$ , final time  $T = 12$ ,  $\kappa = 20$ ,  $\beta = 1$ , relative adhesion coefficient  $\sigma = -0.78$ , merging threshold  $\varepsilon = 0.01$ , Bond number  $Bo = 0.0832$  for Droplet 1 and  $Bo = 0.7861$  for Droplet 2, initial Droplet 1 profile (magenta double-dotted line) given in (4.8) with  $a(0) = 1.9, b(0) = 2.2$  and initial Droplet 2 profile (green double-dotted line) given in (4.9) with  $a(0) = 2.4, b(0) = 2.9$ . (upper) Droplet 1 with slow capillary rise; (middle) Droplet 2 moves down fast due to gravitational effect; (down) Dynamics of two droplets: merge together and then moves down as a new big droplet with final profile shown in solid blue lines.

## ACKNOWLEDGE

The authors would like to thank Prof. Tom Witelski for some helpful suggestions. J.-G. Liu was supported in part by the National Science Foundation (NSF) under award DMS-1812573.

## REFERENCES

- [1] L. Almeida, A. Chambolle, and M. Novaga. Mean curvature flow with obstacles. *Annales de lInstitut Henri Poincaré (C) Non Linear Analysis*, 29(5):667681, Sep 2012.
- [2] L. Ambrosio, N. Gigli, and G. Savar. *Gradient flows: in metric spaces and in the space of probability measures*. Lectures in mathematics ETH Zrich. Birkhäuser, 2005.
- [3] W. Böhm, G. Farin, and J. Kahmann. A survey of curve and surface methods in cagd. *Computer Aided Geometric Design*, 1(1):1–60, 1984.
- [4] H. Brezis. Opérateurs maximaux monotones: et semi-groupes de contractions dans les espaces de hilbert. 1973.
- [5] L. A. Caffarelli, K.-A. Lee, and A. Mellet. Homogenization and flame propagation in periodic excitable media: the asymptotic speed of propagation. *Communications on Pure and Applied Mathematics: A Journal Issued by the Courant Institute of Mathematical Sciences*, 59(4):501–525, 2006.
- [6] L. A. Caffarelli and A. Mellet. Capillary drops: Contact angle hysteresis and sticking drops. *Calculus of Variations and Partial Differential Equations*, 29(2):141160, Mar 2007.
- [7] L. A. Caffarelli and A. Mellet. *Capillary drops on an inhomogeneous surface*, volume 446, page 175201. American Mathematical Society, 2007.
- [8] X. Chen, X.-P. Wang, and X. Xu. Effective contact angle for rough boundary. *Physica D: Nonlinear Phenomena*, 242(1):5464, Jan 2013.
- [9] A. J. Chorin. On the convergence of discrete approximations to the navier-stokes equations. *Mathematics of computation*, 23(106):341–353, 1969.
- [10] S. H. Davis. Moving contact lines and rivulet instabilities. part 1. the static rivulet. *Journal of Fluid Mechanics*, 98(2):225242, May 1980.
- [11] P.-G. De Gennes, F. Brochard-Wyart, and D. Quéré. *Capillarity and wetting phenomena: drops, bubbles, pearls, waves*. Springer Science & Business Media, 2013.
- [12] S. Esedoglu and F. Otto. Threshold dynamics for networks with arbitrary surface tensions. *Communications on Pure and Applied Mathematics*, 68(5):808864, May 2015.
- [13] S. Esedoglu, R. Tsai, and S. Ruuth. Threshold dynamics for high order geometric motions. *Interfaces and Free Boundaries*, page 263282, 2008.
- [14] W. M. Feldman and I. C. Kim. Dynamic Stability of Equilibrium Capillary Drops. *Arch Rational Mech Anal*, 211(3):819–878, Mar. 2014.
- [15] W. M. Feldman and I. C. Kim. Liquid drops on a rough surface. *Communications on Pure and Applied Mathematics*, 71(12):24292499, Dec 2018.
- [16] Y. Gao and J.-G. Liu. Gradient flow formulation and second order numerical method for motion by mean curvature and contact line dynamics on rough surface. *arXiv preprint arXiv:2001.04036*, 2020.
- [17] R. Glowinski, J.-L. Lions, and R. Trémolières. *Numerical analysis of variational inequalities*. Studies in mathematics and its applications. North-Holland Pub. Co.; Sole distributors for the U.S.A. and Canada, 1981.
- [18] H. Goldstein, C. Poole, and J. Safko. Classical mechanics. 3rd, 2002.
- [19] N. Grunewald and I. Kim. A variational approach to a quasi-static droplet model. *Calculus of Variations and Partial Differential Equations*, 41(12):119, May 2011.
- [20] W. Jiang, W. Bao, C. V. Thompson, and D. J. Srolovitz. Phase field approach for simulating solid-state dewetting problems. *Acta Materialia*, 60(15):55785592, Sep 2012.
- [21] T. Kato and K. Masuda. Trotters product formula for nonlinear semigroups generated by the subdifferentials of convex functionals. *Journal of the Mathematical Society of Japan*, 30(1):169178, Jan 1978.
- [22] I. Kim and A. Mellet. Liquid drops sliding down an inclined plane. *Transactions of the American Mathematical Society*, 366(11):61196150, May 2014.

- [23] Y. KOMURA. Nonlinear semi-groups in hilbert space. *Journal of the Mathematical Society of Japan*, 19(4):493–507, 1967.
- [24] S. Leung and H. Zhao. A grid based particle method for moving interface problems. *Journal of Computational Physics*, 228(8):29933024, May 2009.
- [25] P. L. Lions and B. Mercier. Splitting algorithms for the sum of two nonlinear operators. *SIAM Journal on Numerical Analysis*, 16(6):964979, Dec 1979.
- [26] G. Mercier and M. Novaga. Mean curvature flow with obstacles: existence, uniqueness and regularity of solutions. *Interfaces and Free Boundaries*, 17(3):399–427, 2015.
- [27] L. W. Morland. A fixed domain method for diffusion with a moving boundary. *Journal of Engineering Mathematics*, 16(3):259269, Sep 1982.
- [28] K. W. P.A. *Riemannian Geometry*. De Gruyter, 2011.
- [29] T. Qian, X.-P. Wang, and P. Sheng. A variational approach to moving contact line hydrodynamics. *Journal of Fluid Mechanics*, 564:333, Oct 2006.
- [30] R. Scholz. Numerical solution of the obstacle problem by the penalty method. *Computing*, 32(4):297306, Dec 1984.
- [31] R. Temam. Quelques méthodes de décomposition en analyse numérique. In *Actes Congrès Intern. Math*, pages 311–319, 1970.
- [32] G. Tran, H. Schaeffer, W. M. Feldman, and S. J. Osher. An  $l^1$  penalty method for general obstacle problems. *SIAM Journal on Applied Mathematics*, 75(4):14241444, Jan 2015.
- [33] C. Villani. *Optimal transport: old and new*. Grundlehren der mathematischen Wissenschaften. Springer, 2009.
- [34] D. Wang, X.-P. Wang, and X. Xu. An improved threshold dynamics method for wetting dynamics. *Journal of Computational Physics*, 392:291310, Sep 2019.
- [35] Y. Wang, W. Jiang, W. Bao, and D. J. Srolovitz. Sharp interface model for solid-state dewetting problems with weakly anisotropic surface energies. *Physical Review B*, 91(4):045303, Jan 2015. arXiv: 1407.8331.
- [36] E. Weinan and X.-P. Wang. Numerical methods for the landau-lifshitz equation. *SIAM journal on numerical analysis*, pages 1647–1665, 2001.
- [37] X. Xu, Y. Di, and M. Doi. Variational method for contact line problems in sliding liquids. *Phys. Fluids*, 28:087101, 2016.
- [38] T. Young. Iii. an essay on the cohesion of fluids. *Philosophical transactions of the royal society of London*, (95):65–87, 1805.
- [39] H.-K. Zhao, T. Chan, B. Merriman, and S. Osher. A variational level set approach to multiphase motion. *Journal of Computational Physics*, 127(1):179195, Aug 1996.
- [40] D. Zosso, B. Osting, M. Xia, and S. J. Osher. An efficient primal-dual method for the obstacle problem. *Journal of Scientific Computing*, 73(1):416437, Oct 2017.